Supporting Information

On the photostability and luminescence of dye-sensitized upconverting nanoparticles using modified IR820 dyes

*Mannu Kaur, Gabrielle A. Mandl, Steven L. Maurizio, Gabriella Tessitore, John A. Capobianco**

Quantification of dye molecules per nanoparticle (Table S1)

Calibration curves were established for each dye sample in the range of 0.5 – 5 µM in methanol. The extinction coefficients for each dye were then obtained and utilized to calculate the observed dye concentrations in the nanoparticle samples which could then be utilized to obtain the number of molecules of dye in solution. The dimensions of the nanoparticles obtained from transmission electron microscopy images were utilized to calculate the volume of a single nanoparticle, and the density of the host material, $NaGdF_4$ (5.61 g/cm^3)[1] was obtained from the literature and combined, these values were utilized to estimate the mass of a single nanoparticle.

Dye concentration added (µM)	Dye conc. linked on NPs x10^{-3}(µM)		# dye molecules linked per particle	
	IR 820	IR 820-NO_2	IR 820	IR 820-NO_2
8	6	5	42	38
12	12	1	80	67
16	15	14	99	94
20	21	18	127	118

Table S1. Quantification of no. of dye molecules linked per nanoparticle.

Photo-degradation of IR820 in the presence of different assays and in different solvents

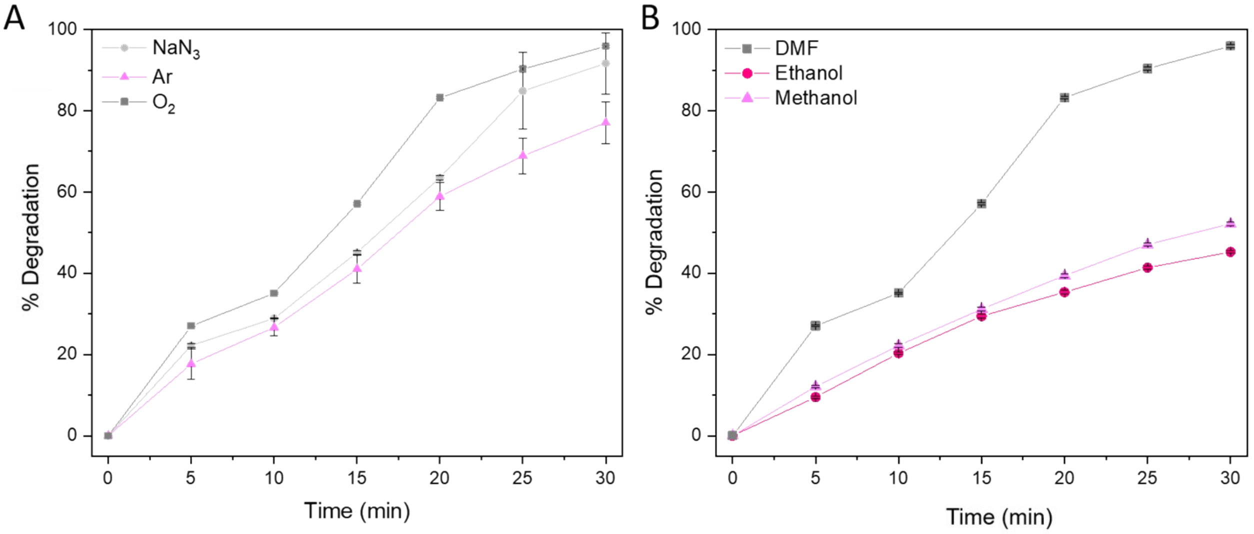

Figure S1. A) Percent degradation of IR820 (16**µ**M in DMF) dye versus time in ambient conditions (gray), in the presence of sodium azide (light gray) and under Ar atmosphere (pink). B) Percent degradation of IR820 dye versus time in DMF (gray), ethanol (dark pink), and methanol (light pink). Errors based on a minimum of three repetitions.

Each assay was performed on a 16 µM solution in the corresponding solvent and a UV-visible absorption spectrum was measured at 5-minute intervals of irradiation with 800 nm light (4.2 W/cm^2). To obtain an inert atmosphere, the solution was purged with Argon for 10 minutes and sealed. Sodium azide was added at a concentration of 50 mM.

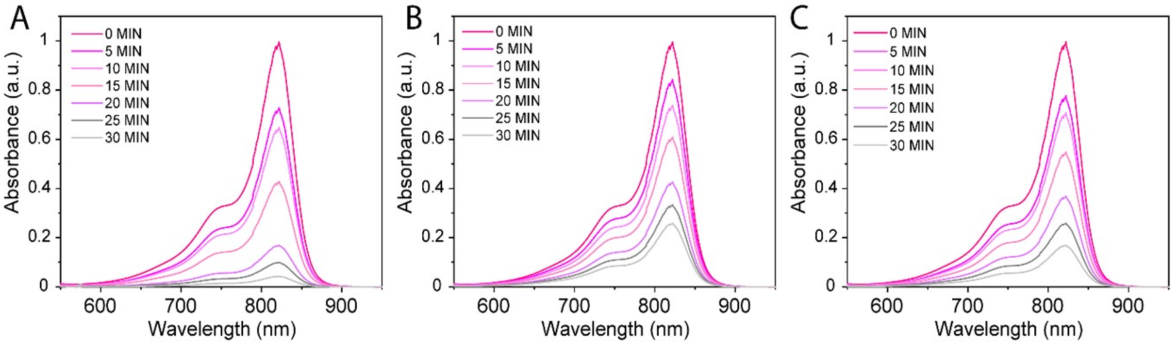

Figure S2. Absorbance of IR820 a) in air b) in Ar atmosphere c) with 50 mM sodium azide added in solution

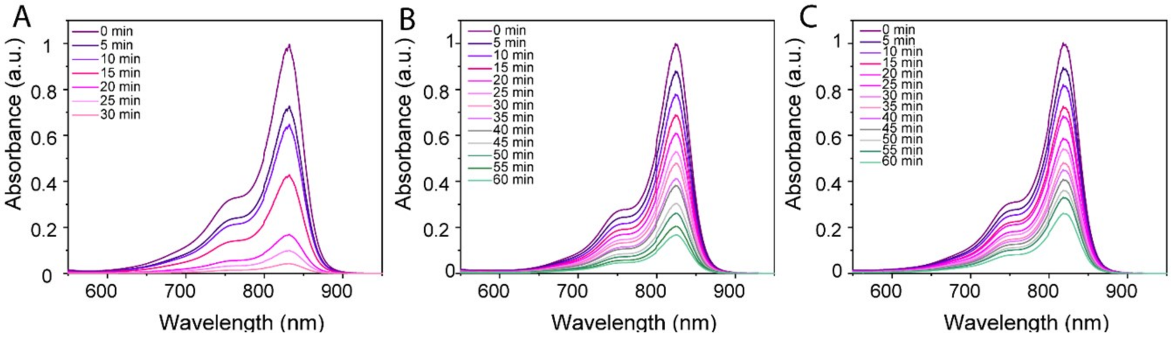

Figure S3. Decrease in absorbance of IR820 with irradiation time in a) DMF b) EtOH c) MeOH

Analysis of photodegradation products of IR820 by ESI-MS

40ug/ml of IR 820 dye was dissolved in DMF and irradiated at 800 nm for 15 minutes. The irradiated sample was analyzed for photoinduced degradation.[2]

Peak	**Molecular weight (MW)**	**Mass to charge ratio (m/z)**
i	369.41[i]	368.03 [i-H+Na]
ii	394.45[iii]	392.01[ii-H+Na]
iii	509.01[ii]	508.17[iii-H+Na]
iv	535.05[iv]	534.21[iv-H+Na]
IR820	871.44[M]	435.58[M]/2

***Table* S2** Mass to charge ratio and molecular weight of peaks determined by ESI-MS analysis.

^{1}H-NMR and MALDI-TOF-MS of IR820 derivatives

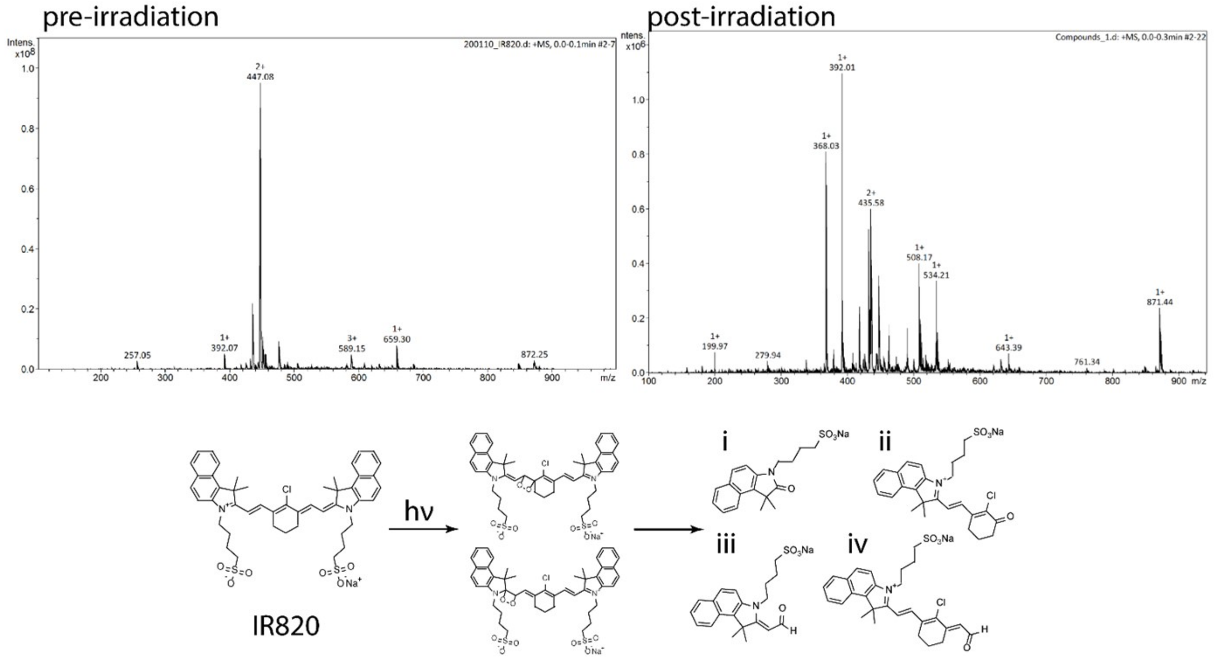

Figure S4. ESI-MS analysis of non-irradiated IR820 ESI-MS analysis and degradation mechanism of irradiated IR 820 (at 800 nm 4.2 W/cm^2).

Synthesis of IR820-CH_3 yielded 87.5 mg (0.0975 mmol, 87%). ^{1}H NMR (500 MHz. d^6-DMSO): δ 8.18(1H d), δ 8.05 (1H d), δ 7.95 (1H d), δ 7.93 (1H d), δ 7.92 (1H d), δ 7.61 (1H d), δ 7.54 (1H t), δ 7.52 (1H t), δ 7.47 (1H d), δ 7.45 (1H t), δ 7.29 (1H t), δ 7.07 (2H d), δ 7.06 (1H d), δ 6.89 (2H d), δ 6.55 (1 H d), δ 6.23 (1H d), δ 5.33 (1H d), δ 5.21 (1H d), δ 4.07 (4H t), δ 2.81 (4H d), δ 2.34 (3H s), δ 1.82 (6H s), δ 1.62 (6H s), δ 1.60 (2H p), δ 1.49 (4H t), δ 1.3 (4H t), MALDI- Calculated for $C_{53}H_{59}N_2O_6S_3$: 915.35; found 915.32.

Synthesis of IR820-COOH: Method same as above with 0.58mmol 4-mercaptobenzoic acid, IR820-COOH 92.5 mg (0.0979 mmol, 89%). ^{1}H NMR (500 MHz. d^6-DMSO): δ 8.18(1H d), δ 8.05 (1H d), δ 8.05 (2H d), δ 7.95 (1H d), δ 7.93 (1H d), δ 7.92 (1H d), δ 7.61 (1H d), δ 7.60 (2H d), δ 7.54 (1H t), δ 7.52 (1H t), δ 7.47 (1H d), δ 7.45 (1H t), δ 7.29 (1H t), δ 7.06 (1H d), δ 6.55 (1H d), δ 6.23 (1H d), δ 5.33 (1H d), δ 5.21 (1H d), δ 4.07 (4H t), δ 2.81 (4H d), δ 1.82 (6H s), δ 1.62 (6H s), δ 1.60 (2H p), δ 1.49 (4H t), δ 1.3 (4H t). MALDI- Calculated for $C_{53}H_{57}N_2O_8S_3$: 945.32; found 945.33

Synthesis of IR820-CF_3: Method same as above with 4-(trifluoromethyl) thiophenol. Yield IR820-CF_3 98 mg (0.101 mmol, 92%). ^{1}H NMR (500 MHz. d^6-DMSO): δ 8.18(1H d), δ 8.05 (1H d), δ 7.95 (1H d), δ 7.93 (1H d), δ 7.92 (1H d), δ 7.61 (1H d), δ 7.54 (1H t), δ 7.52 (1H t), δ 7.47 (1H d), δ 7.45 (1H t), δ 7.29 (1H t), δ 7.23(2H d), δ 7.06 (1H d), δ 6.94 (2H d), δ 6.55 (1 H d), δ 6.23 (1H d), δ 5.33 (1H d), 5.21 (1H d), δ 4.07 (4H t), δ 2.81 (4H d), δ 1.82 (6H s), δ 1.62 (6H s), δ 1.60 (2H p), δ 1.49 (4H t), δ 1.3 (4H t).MALDI- Calculated for $C_{53}H_{56}N_2O_6S_3F_3$: 969.32; found 969.32.

Synthesis of IR820-NO_2: Method same as above with 4-nitrothiophenol. Yield IR820-NO_2 96.8 mg (0.102 mmol, 93%). ^{1}H NMR (500 MHz. d^6-DMSO): δ 8.18(1H d), δ 8.10 (2H d), δ 8.05 (1H d), δ 7.95 (1H d), δ 7.93 (1H d), δ 7.92 (1H d), δ 7.65 (3H t), δ 7.61 (1H d), δ 7.54 (1H t), δ 7.52 (1H t), δ 7.47 (1H d), δ 7.45 (1H t), δ 7.29 (1H t), δ 7.06 (1H d), δ 6.55 (1 H d), δ 6.23 (1H d), δ 5.33 (1H d), δ 5.21 (1H d), δ 4.07 (4H t), δ 2.81 (4H d), δ 1.82 (3H s), δ 1.62 (3H s), δ 1.60(2H p) δ 1.49 (4H t), δ 1.3 (4H t). MALDI- Calculated for $C_{52}H_{56}N_3O_8S_3$: 946.3; found 946.4.

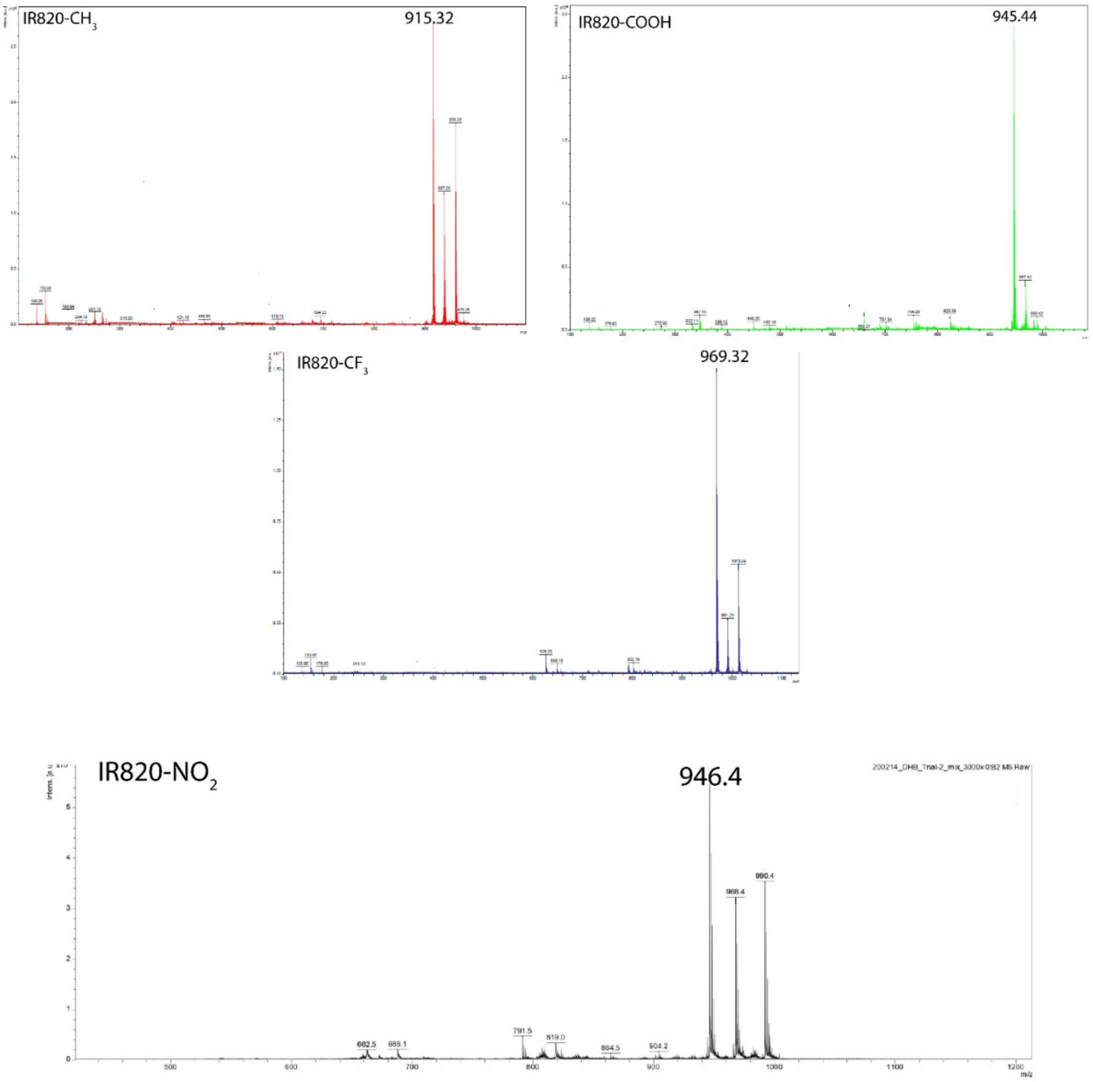

Figure S5. MALDI-TOF analysis of IR820-CH_3 (MW 915.32), IR820-COOH (MW 945.44), IR820-CF_3 (MW 969.32) and IR820-NO_2 (MW 946.4)

UV-Visible absorption spectra of IR820 derivatives and corresponding maxima

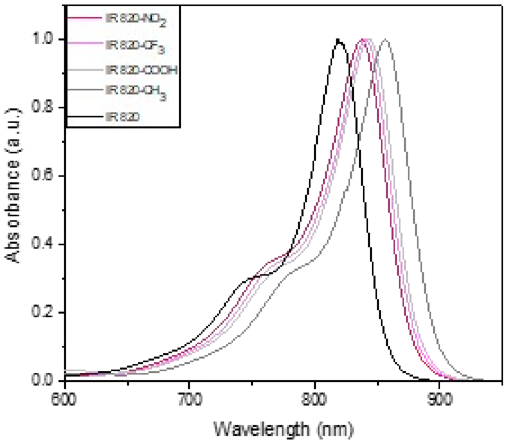

Figure S6. Absorbance of IR820 and IR820 functionalized with thiophenol with different para substituents: IR820 (black), IR820-NO_2(pink), IR820-CF_3(light pink), IR820-COOH(light gray), IR820-CH_3(gray).

Dye	Absorbance λ_{max}(nm)	Emission λ_{max}(nm)
IR820	820	850
IR820-CH_3	850	900
IR820-COOH	845	920
IR820-CF_3	840	945
IR820-NO_2	837	950

Table S3. Absorbance and fluorescence (λ_{ex} 800 nm) of IR820 and functionalized dyes in methanol.

Analysis of photodegradation of IR820 derivatives by UV-Visible absorption spectroscopy

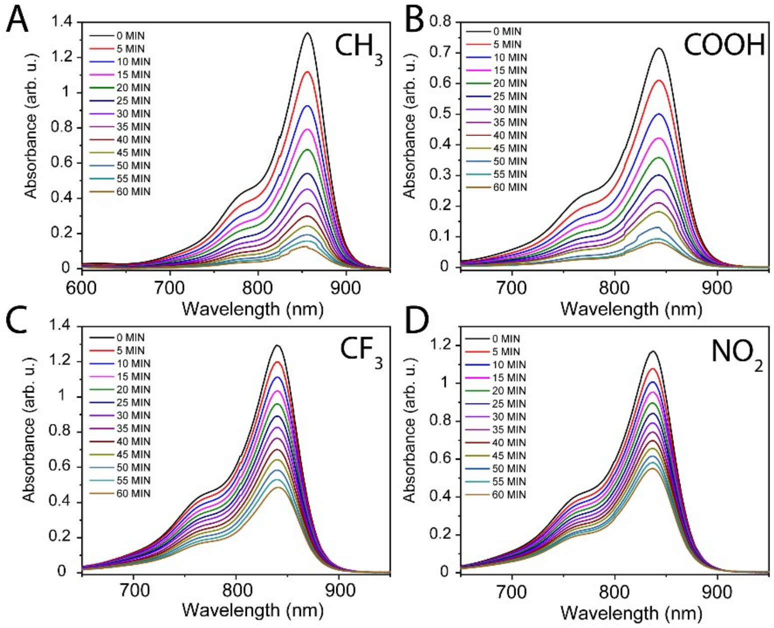

Figure S7. Decrease of absorbance of A) IR820-CH_3 B) IR820-COOH C) IR820-CF_3 and D) IR820-NO_2 with irradiation time.

Physical characterization of core/shell $NaGdF_4:Yb^{3+},Er^{3+}/NaGdF_4:Yb^{3+}$ nanoparticles

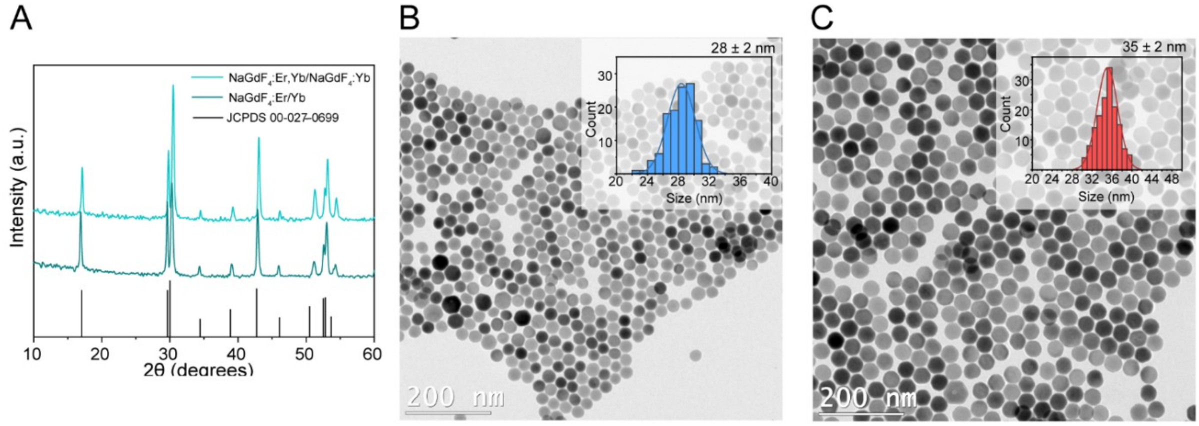

Figure S8. A) X-ray powder diffraction pattern of $NaGdF_4:Er^{3+}(2\%),Yb^{3+}(20\%)/NaGdF_4:Yb^{3+}(20\%)$ (core/shell) and $NaGdF_4:Er^{3+}(2\%),Yb^{3+}(20\%)$ (core) nanoparticles B) TEM image of a) $NaGdF_4$: Yb^{3+},Er^{3+} (cores) C) $NaGdF_4:Yb^{3+},Er^{3+}/NaGdF_4:Yb^{3+}$ (core/shell) nanoparticles

FT-IR spectra for characterization of nanoparticle surface

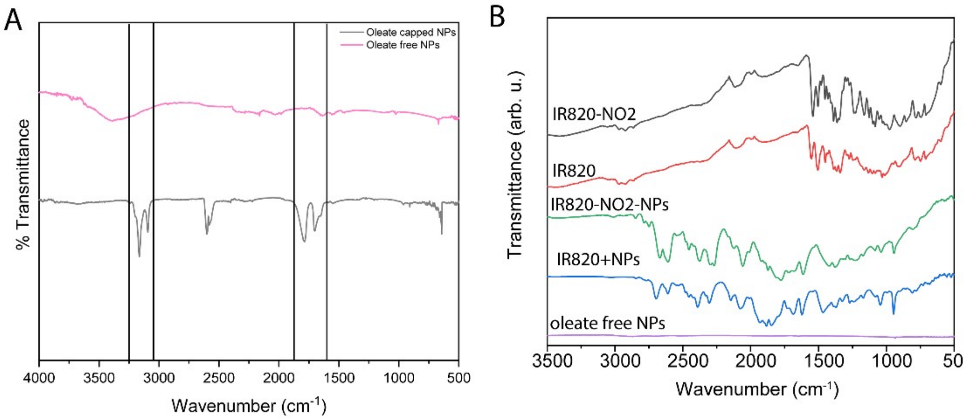

Figure S9. FT-IR of A) oleate capped and oleate free nanoparticles. Absence of peaks 3300 cm^{-1} and 1700 cm^{-1} in oleate free nanoparticles, confirms removal of oleate B) Dye and nanoparticles conjugated with the respective dye.

The FT-IR reveals the emergence of bands at 3000 cm^{-1} (C=C from dye), 1375 cm^{-1}(C=C bending), 1260 cm^{-1}(C-N stretching), and 1100 cm^{-1} (S=O stretching) in UCNPs functionalized with dyes. Additionally, a slight red shift (70 cm^{-1}) is observed in the S=O stretching vibration(1170 cm^{-1}) upon conjugation of the dye to the LnUCNP surface, compared to the dye itself (1170 cm^{-1}), which indicates that the electron density of the sulfonate group is being shared with positively charged nanoparticle surface, thereby weakening the S-O bonds and shifting the vibration maximum to a lower wavenumber.[3]

Transmission Electron Microscopy images of oleate-free nanoparticles

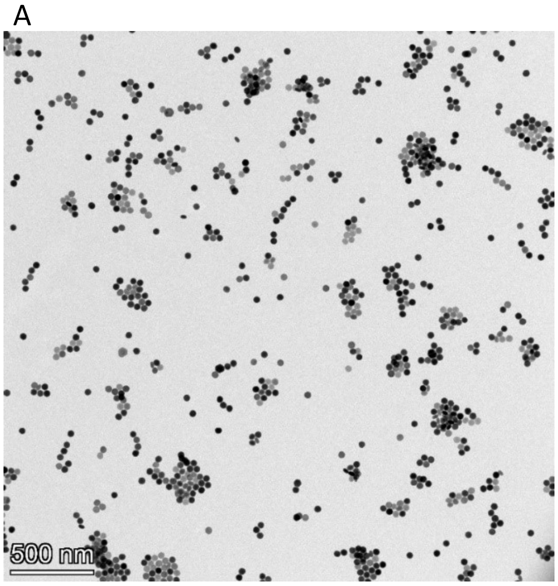

Figure S10 A. Transmission electron microscopy images of oleate-free LnUCNPs. 1 mg/mL dispersion in ethanol.

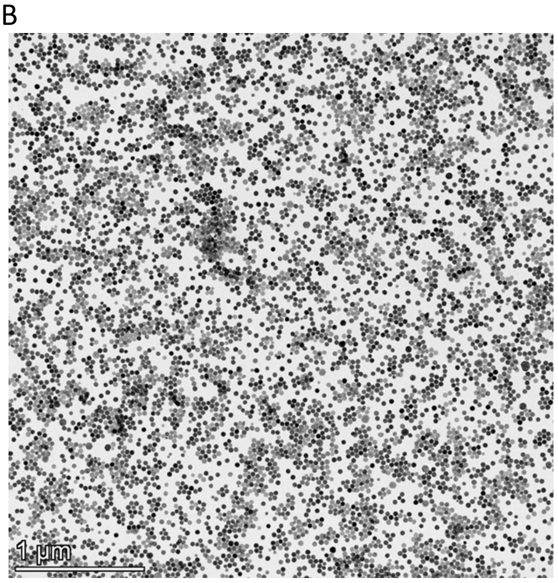

Figure S10 B. Transmission electron microscopy image of IR820-NO_2 LnUCNPs 1 mg/ml dispersion in methanol

Calibration curves for quantification of number of dye molecules per nanoparticle

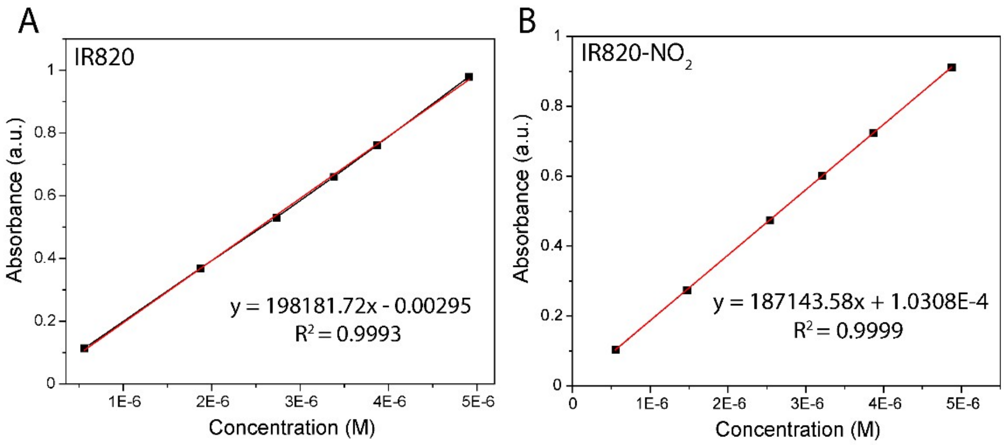

Figure S11. Calibration curve of A) IR820 and B) IR820-NO_2 having 198181 M^{-1} cm^{-1} and 187143 M^{-1} cm^{-1} molar extinction coefficients in methanol, respectively.

Emission Spectra of IR820 and IR820-NO_2 functionalized NPs at different dye concentrations

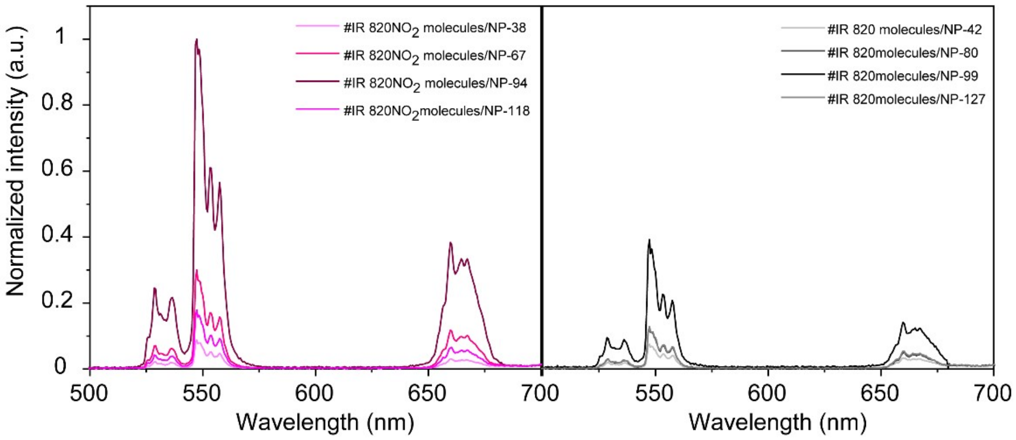

Figure S12. Emission spectra of IR820-NO_2 (pink) and IR820 (gray) functionalized UCNPs (in MeOH) having different dye concentrations and 10mg/ml UCNPs excited at 800 nm (2.1 W/cm^2)

Stability study on electrostatic interaction of IR820-NO_2 dye with NP surface

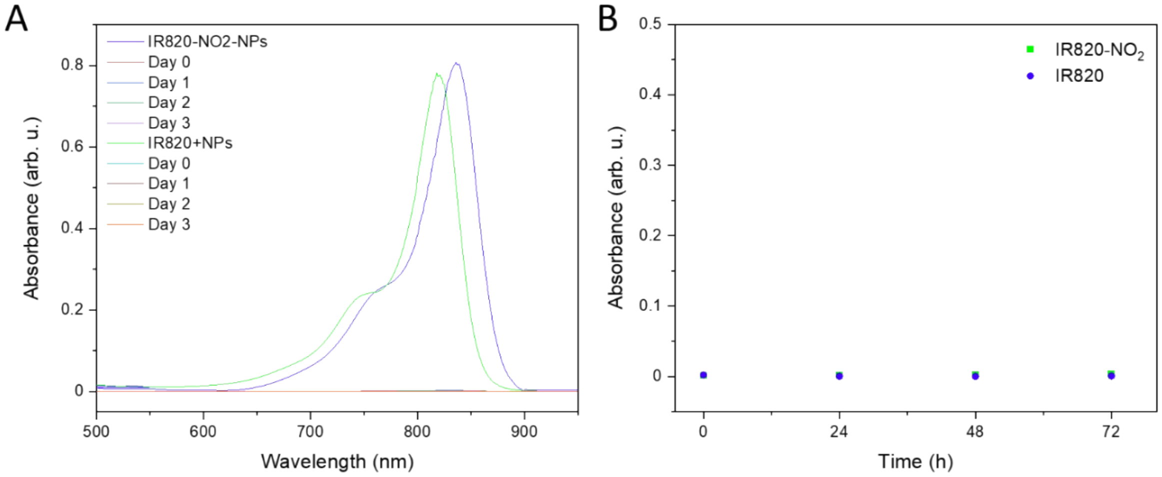

Figure S13. A) UV-visible absorption spectrum of supernatant collected after 24, 48 and 72 h from a dispersion of IR820-NO_2-LnUCNPs (10 mg/mL) in MeOH. B) Absorption of supernatant of a dispersion of IR820-LnUCNPs at 820 nm and IR820-NO_2-LnUCNPs at 837 nm as a function of time. No leakage of dye from the nanoparticle surface was observed.

Kinetics of IR820-NO_2 degradation with $NaGdF_4:Er^{3+}/Yb^{3+}$ and $NaYF_4:Er^{3+}/Yb^{3+}$

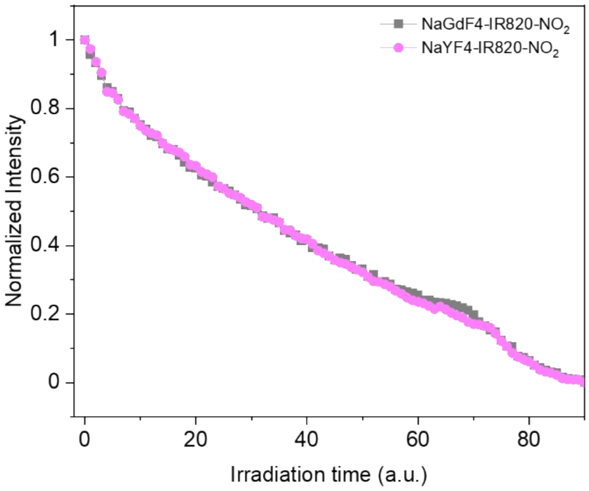

Figure S14. Normalized green emission intensity of LnUCNPs versus irradiation time for $NaGdF_4$-IR820-NO_2 (gray) and $NaYF_4$-IR820-NO_2 (pink) under 800 nm excitation (at 4.2 W/cm^2).

Upconversion emission spectra comparisons upon different excitation wavelengths

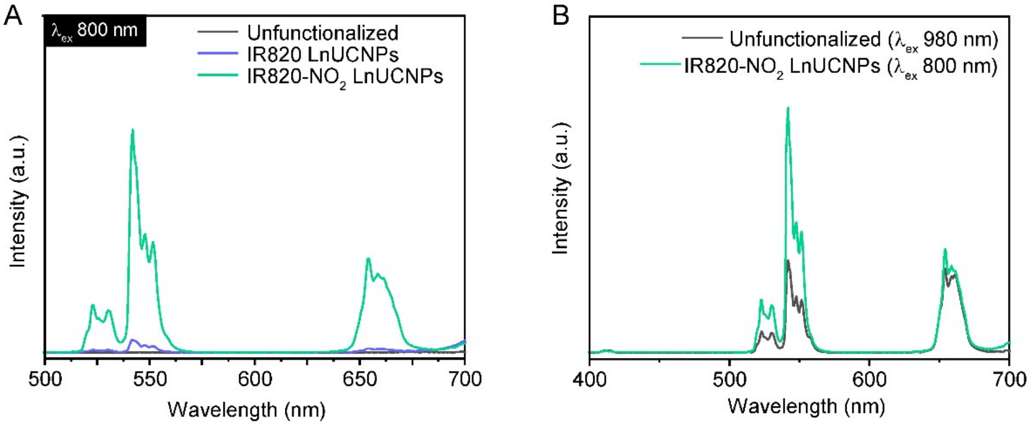

Figure S15. A) Upconversion emission spectra of colloidal dispersions of unfunctionalized LnUCNPs (gray), IR820 LnUCNPs (blue) and IR820-NO$_2$ LnUCNPs (green) upon 800 nm excitation (2.1 W/cm^2). B) Upconversion emission spectra of colloidal dispersions of unfunctionalized LnUCNPs (gray) and IR820-NO$_2$ LnUCNPs (green) upon 980 nm excitation and 800 nm excitation, respectively (both at power densities of 4.2 W/cm^2).

Calibration curves for absorption coefficients at 655 nm

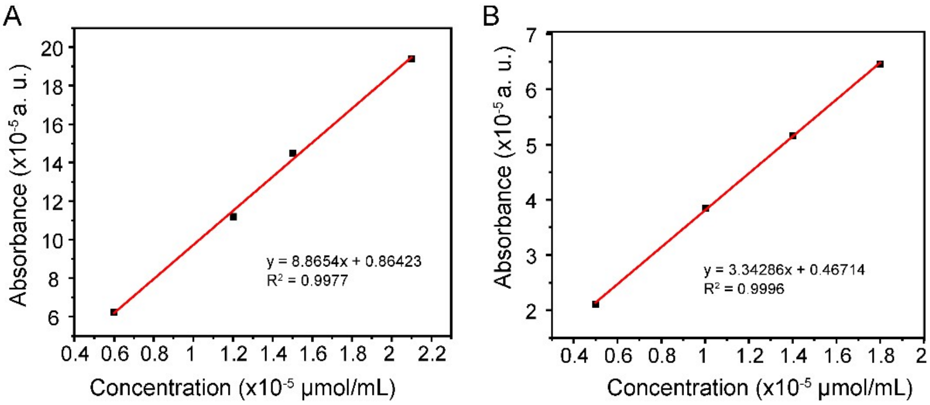

Figure S16. A) Calibration curve for IR820 at 655 nm in methanol B) Calibration curve for IR820-NO_2 at 655 nm in methanol

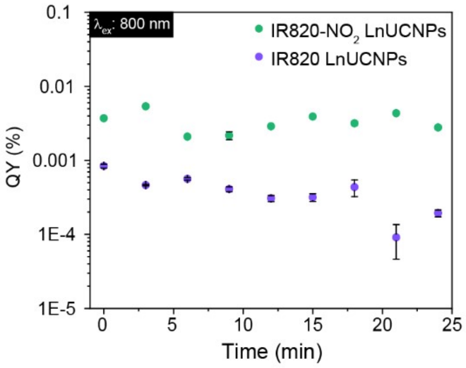

Figure S17. Quantum yields of IR820-NO_2-LnUCNPs (green) and IR820-LnUCNPs (blue) as a function of irradiation time upon 800 nm excitation. Errors for both measurements established based on a minimum of two repetitions.

1 N. Liu, R. Marin, Y. Mazouzi, G. O. Cron, A. Shuhendler and E. Hemmer, *Nanoscale*, 2019, **11**, 6794–6801.

2 R. R. Nani, J. A. Kelley, J. Ivanic and M. J. Schnermann, *Chem. Sci.*, 2015, **6**, 6556–6563.

3 X. Wu, H. Lee, O. Bilsel, Y. Zhang, Z. Li, T. Chen, Y. Liu, C. Duan, J. Shen, A. Punjabi and G. Han, 2015,**7**, 18424–18428.